Wind farm response to mesoscale-driven coastal low level jets: a multiscale large eddy simulation study

Tanmoy Chatterjee[1], Jing Li[1], Shashank Yellapantula[2], Balaji Jayaraman[1] and Eliot Quon[2]

[1] GE Research, 1 Research Circle, Niskayuna, NY - 12309 , [2] National Renewable Energy Laboratory, 15013 Denver West Parkway, Golden, CO 80401, USA.

E-mail: tanmoy.chatterjee@ge.com, balaji.jayaraman@ge.com

Abstract.

Realistic atmospheric turbulence–wind farm interactions during coastal low-level jet (LLJ) events are captured using high-fidelity, mesoscale-driven large eddy simulations (LES) to understand wind turbine loads, wakes and overall performance. The simulation has been carried out using the ExaWind aeroelastic solver, AMR-Wind. The simulations have been compared against a baseline unstable case matching the wind speed, wind direction and TI at hub-height location. Results indicate that the LLJ has negative impacts on the turbine hub and tower loads, and opens up potential avenues for design load mitigation strategies.

1. Introduction

With advances in computational power, wind energy research has progressively leveraged high-fidelity simulations of atmospheric turbulence and their multiscale interactions with wind turbines for design considerations. Until recently, most of these coupled studies such as [1, 2] focused on the interaction of canonical atmospheric turbulence (with well-known structural characteristics [3]) with wind turbines. While they represent foundational analyses within the field, the findings do not always translate to operational settings. With advances in modeling of mesoscale-driven atmospheric turbulence (see companion paper #651), it is increasingly feasible to model non-stationary turbulence events such as low-level jets and their interaction with wind farms. Low-level jets (LLJs) can be seen in the atmosphere when the boundary layer is stably stratified and are an important wind phenomenon both to the climate and wind energy community [4, 5]. A coastal LLJ is a mesoscale-driven wind event associated with a non-monotonic wind profile whose maximum velocity occurs at the so-called "jet nose," with a strong positive shear below the nose and a negative shear above it. Our recent work based on lidar measurements within the lowest 200 m of the marine atmospheric boundary layer (ABL) in the New York Bight found that LLJs occur at least 2-7% of the time in a year depending on what LLJ detection criteria were used. Despite that, an LLJ is a non-conventional wind event whose characteristics are not well understood and is currently not considered in the annual energy production (AEP) calculations from engineering models and Reynolds-averaged Navier–Stokes solvers (RANS) [6]. Recent work has used LES to create a synthetic LLJ event for studying their impact on wind farms. However, the study focused mainly on the energy harvest and AEP influenced by the LLJ nose height and turbulence [7]. The present work aims to characterize LLJs

using more realistic mesosale-driven events and understand the impact of LLJs on wind turbines using high-fidelity LES that simultaneously computes turbine performance and loads. We exercise high-fidelity predictive tools in the ExaWind software stack [8], in particular the AMR-Wind/OpenFAST fluid-structure coupled modeling environment, to simulate the atmospheric and wind farm flow. We focus our study on the marine ABL of the US North Atlantic coast, specifically an area within a wind energy call areas in the New York Bight where a set of floating lidar buoy measurements were made available by the New York State Energy Research and Development Authority (NYSERDA) [9].The IEA 15-MW offshore reference wind turbine [10] was considered, which represents the size and capacity of current and near-future designs.

2. Methodology

2.1. Atmospheric flow modeling

A Mesoscale-to-Microscale Coupling (MMC) approach based on offline dynamic internal forcing [11] was adopted to simulate a realistic coastal LLJ event. First, we analyzed the NYSERDA dataset over a year. A mesoscale simulation was performed over the same period using the Weather and Research Forecasting (WRF) model, using the model configuration of [12]. For an LLJ event that occurred on May 15, 2020, we obtained a WRF result that was in excellent agreement with the observation (Figure 1). Then, we performed an LES in AMR-Wind to resolve the microscale turbulence processes during the LLJ event (10 metre resolution) in a 12-hr window, based on a combination of direct and indirect assimilation [11] of the time–height varying WRF mesoscale wind and potential temperature profiles respectively, extracted from the geographic location nearest to the buoys. This MMC approach is based on the assumption of horizontal homogeneity, i.e., the spatial scales of resolved coastal features being on the order of the microscale domain extent or larger. Past research showed that this assumption is valid for onshore nocturnal LLJ [11, 13]

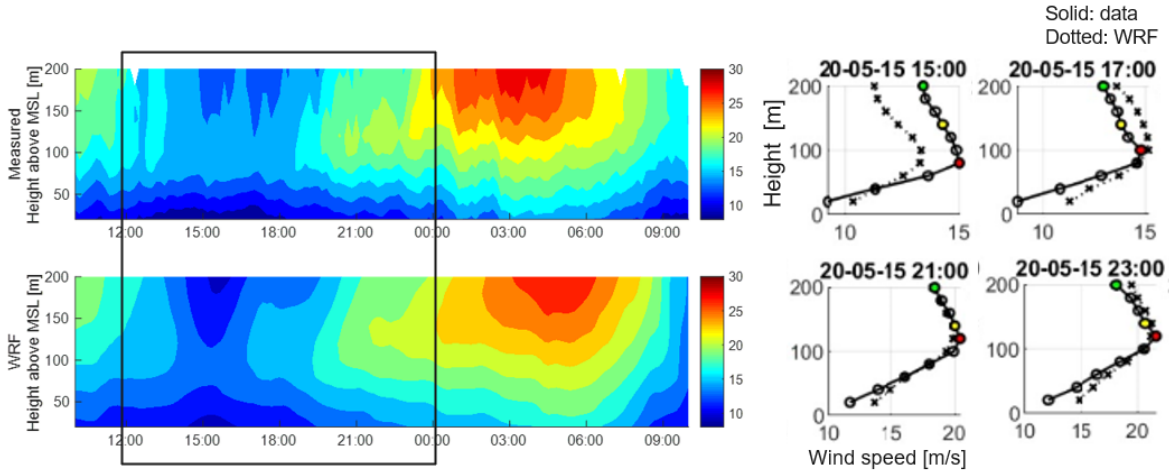

Figure 1: Left: Time-height contour plots of wind speed. Top panel is the lidar buoy measurement (South Buoy). Bottom panel is the WRF prediction. The black box indicates time range on which AMR-Wind microscale LES was carried out. Right: 10-min averaged wind speed profiles at four time instances. Solid lines are observations. Dotted lines are WRF predictions.

Case	Domain Size	Mesh Count [$\times 10^6$]
MS (baseline, precursor)	5km $\times$ 5km $\times$ 2km	67
MS (baseline, ALM : 1WT)	5km $\times$ 5km $\times$ 2km	246
MS (baseline, ALM : 20WT)	10km $\times$ 10km $\times$ 2km	1500
LLJ (precursor)	5km $\times$ 5km $\times$ 1km	34
LLJ (ALM)	5km $\times$ 5km $\times$ 1km	212
LLJ (baseline, ALM : 20WT)	10km $\times$ 10km $\times$ 1km	1400

Table 1: Domain size and mesh count (millions of computational cells) of baseline MS and coastal LLJ simulations (precursor and ALM).

2.2. Wind farm flow modeling

The atmospheric flow simulation discussed above was used as a precursor to wind farm flow simulations. For the LLJ event comprising of a 12 hr window of mesoscale forcing driven LES simulations, a 20-minute sub-window was identified where a relatively constant plateau of wind speed and direction ($\sim$ 11 m/s, $\sim$ 220 deg) was observed. The wind farm simulations were carried out using inflow and mesoscale forcing generated from the 20-minute window of WRF-driven LES. Turbines were modeled as aero-hydro-servo-elastically coupled systems by OpenFAST and were represented with an actuator line model (ALM) in AMR-Wind. The wake fields and turbine response were computed simultaneously at a spatiotemporal resolution of 2.5 metres ($0.01D$, D: turbine rotor diameter) and 0.0125 s (80 Hz). The turbine response was recorded in the last 10 minutes of the simulation for statistical analysis when the wakes have been fully developed and the turbine internal boundary layer has reached equilibrium. In the present work, a detailed analysis of the single-turbine loads and flow field has been considered along with useful insights extended to the 20-turbine array. In an effort to understand the impact of LLJs on wind farm wakes and turbine performance, the results have been compared against a baseline case of unstable ABL with monotonically sheared wind (MS). The baseline case was designed in an iterative fashion such that it matches the hub-height wind speed, wind direction and TI of the coastal LLJ event. This is based on the hypothesis that the TI at hub-height is an important feature to match for comparison of the loads and is also inline with the industrial standard. However, an alternative approach to the problem involves matching the shear, wind veer and turbulent structure which might also provide useful insights towards load comparison. The second approach would potentially involve a stable boundary layer as baseline case and will be considered subsequently in the future work.

3. Results

We have set up and performed simulations for a single turbine and a 20 wind turbine array ($5D$ longtitudinal spacing, $4D$ lateral spacing), with the yaw of all turbines aligned with the time-averaged hub-height wind direction. The generated power and turbine loads were predicted by the coupled OpenFAST solver. Results have been compared to quantify the difference in power production and fatigue load of turbines, as well as the single- and multi-wake characteristics, between the baseline MS and the LLJ conditions.The domain sizes and mesh count of the precursor ABL and wind turbine simulations are illustrated in Table 1. Note, for the baseline MS case, the vertical domain extent is 2 km as opposed to 1 km in LLJ (stable boundary layer). This is to accommodate the growth of the capping inversion layer owing to the buoyant convective plumes in the unstable layer.

3.1. Precursor Simulations

In this section, we compare the precursor ABL simulations for the LLJ and baseline MS cases. Table 2 compares the integrative quantities u_* (friction velocity), w_* (buoyancy velocity), z_i (inversion height) , L (Monin Obukov length scale, Q (kinematic heat flux) and, wind conditions at hub height (z=150 meters) including wind speed, direction and turbulence intensity (TI). The inversion height is calculated as $z_i = z|_{\overline{\langle w'\theta' \rangle}=0}$ where $\overline{\#}$and$\langle \# \rangle$ denote time and horizontal average respectively. Note, $u_* = \sqrt{\tau_w/\rho}$, where τ_w is the wall shear stress, ρ is air-density and $w_* = sgn(Q)(\frac{g}{\theta_0}|Q|z_i)^{1/3}$, where $sgn(Q)$ is the sign of kinematic wall heat flux. The TI is defined as $TI = \overline{M'M'}/\overline{M}$, where $M = \sqrt{u^2 + v^2}$, is the horizontal wind speed and $M', \overline{M}$, are the fluctuating and mean components of the wind-speed, respectively. Note, this definition of TI is consistent in both atmospheric science community and wind-resource assessment and has been used for matching the wind conditions at hub height between the LLJ and the MS cases. However, we also report $TI_{IEC} = \sigma_{long}/\overline{M_{hub}}$, which is used in the wind energy community for "loads certification", where σ_{long} is the standard deviation of the fluctuating component of the longitudinal velocity. It is critical to note that for coastal LLJ, $z_i/L = 5.25$, while for the MS case, $z_i/L = -22.27$. This indicates that the coastal LLJ is weakly stable while the MS case is strongly unstable.

Case	z_i[m]	Q[m-K/s]	u_*[m/s]	w_*[m/s]	L[m]	$wspd$[m/s]	$wdir$[deg]	TI[-]	TI_{IEC}[-]
MS	1485.0	0.19	0.555	1.54	-66.66	11.86	219.93	11.2	9.58
LLJ	405	-0.01403	0.247	-0.429	77.14	11.75	220.50	13.07	13.07

Table 2: Comparison of time-averaged (20 minute window) integrative quantities and hub-height winds of baseline MS and coastal LLJ case. Variables wsp [m/s], $wdir$[deg],TI,TI_{IEC} are defined at hub-height $z_h = 150.0$ metres.

The time-averaged profile of the ABL precursor is shown in Figure 2. The wind speed illustrates that we match the wind conditions at hub height between the MS and LLJ cases. The 20-minute averaged nose-height of LLJ is 85 meters. Additionally, beyond $z > 400$ meters, the wind speeds from both the cases are similar as they are dominantly geostrophic in nature. This is further corroborated by Figure 3, where we observe significant reduction in both resolved ($k_{resol} = 1/2(\overline{u'^2 + v'^2 + w'^2})$) and subgrid scale ($k_{sgs}$) turbulent kinetic energy beyond $z \sim 400$ metres. What is interesting is that we see relatively consistent wind direction in the unstable MS case, while strong veer (40° across the rotor) persists for the LLJ case. The presence of strong veer is reflected in the turbine loads as discussed in Sections 3.3 and 3.5. The vertical TI_{IEC} profile illustrates that in the near-wall region, $\sim 5\%$ increased TI is observed in the LLJ case (with strong $\frac{\mathrm{d}}{\mathrm{d}z}(TI_{IEC})$) compared to the MS case. Despite stronger rotor region turbulence (TI_{IEC}) in the LLJ case, results in the following section denotes that the presence of wind speed and veer have the most dominant influence on the turbine loads. The potential temperature profile illustrates the presence of a shallow capping inversion later ($z_i \sim 400$ metres) in the LLJ case which is also demonstrated in Table 2.

3.2. Single wind turbine ALM

In this section, we discuss the single-turbine actuator line simulations driven by the ABL precursor as inflow conditions. Figure 4 shows the planform view of the wake propagation of the single turbine at hub-height. For the baseline MS case, the wakes recover quickly due to the vigorous mixing in presence of convective buoyant plumes while in the LLJ case we observe longer recovery regions associated with absence of mixing in the shallow stable layer.

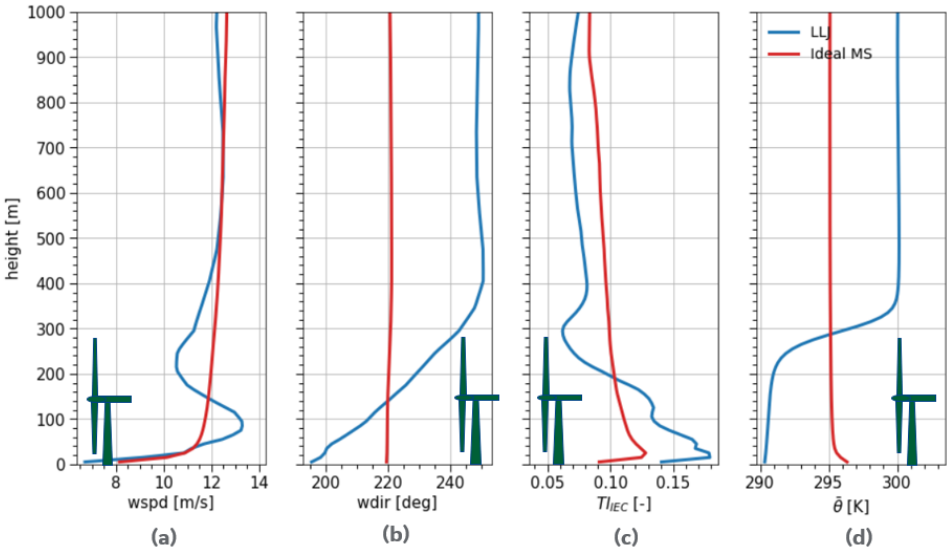

Figure 2: Comparison of time-averaged profile (30 min sampling time-window) of the MS (baseline) and coastal LLJ, with mesoscale forcing driven LES. Metrics: (a) Wind speed, (b) Wind direction or veer, (c) TI [IEC-61400-1] and, (d) Potential Temperature

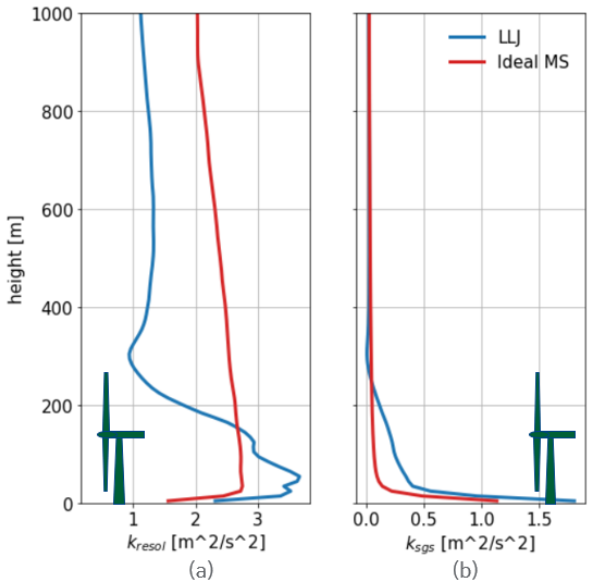

Figure 3: Comparison of time-averaged profile (30 min sampling time-window) of the MS (baseline) and coastal LLJ,with mesoscale forcing driven LES. Metrics: (a) resolved turbulent kinetic energy $\frac{1}{2}(\overline{u'^2} + \overline{v'^2} + \overline{w'^2})$, (b) subgrid scale turbulent kinetic energy

Additionally, we observe distortion of wake structures in the LLJ case that can perhaps be attributed to the strong veer. The presence of wake dispersion is unique to LLJ and was also not observed in recent works of similar high fidelity spectral element simulations of neutral boundary layers of wind farm wakes without veer [14, 15]. However, further studies using the turbulence kinetic energy (TKE) budget is necessary to validate the hypothesis.

Figure 5 illustrates the time-averaged out-of-plane contours of the turbine wake propagation for the LLJ and MS cases. From the figures we observe longer wake recovery lengths and stronger

induction region in the LLJ cases compared to the MS cases which is corroborated from the time-averaged profile plots (wind speed, TI) in Figure 2. Additionally, the augmentation of wake turbulence near the tips of the rotors (strongest production) are observed and is stronger in the MS case compared to the LLJ case.

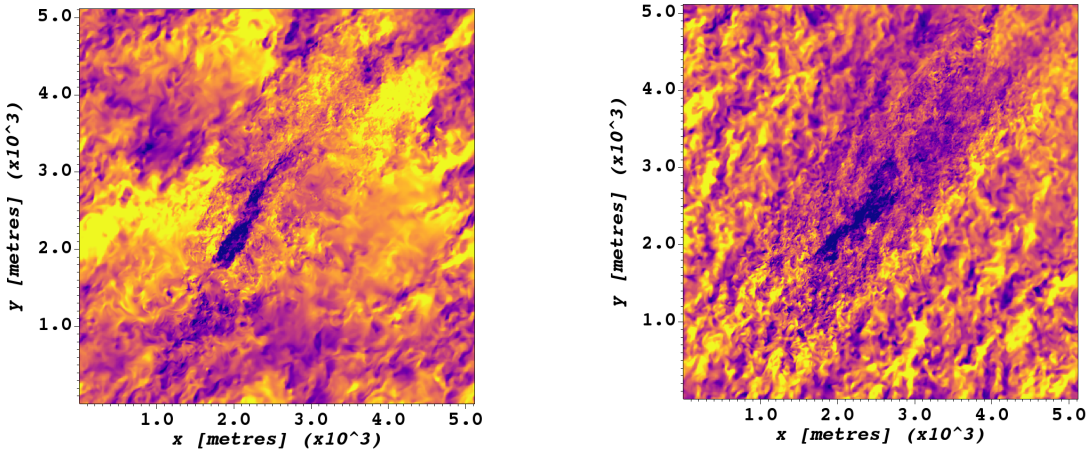

Figure 4: Comparison of instantaneous snapshots (planform view) of wind farms in MS (baseline) (a) and coastal LLJ (b). Colormap same as in Figure 3. Timestamp = 17 minutes

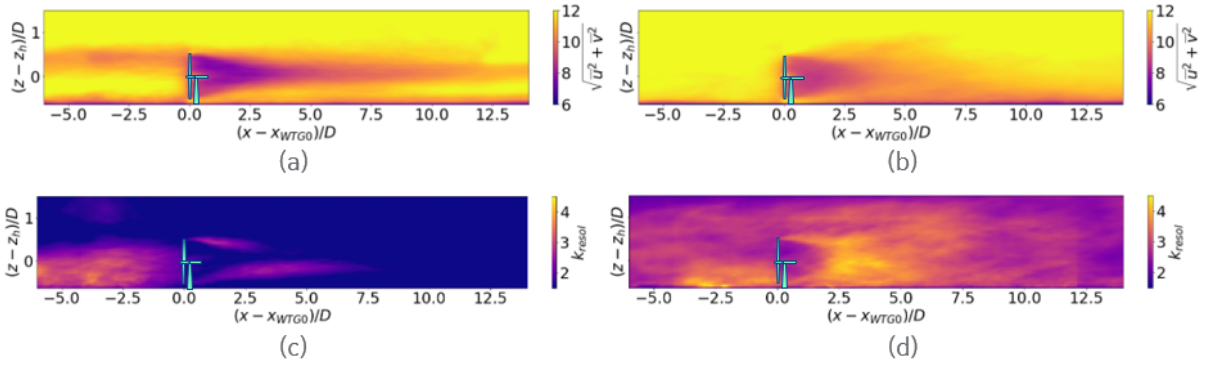

Figure 5: Comparison of time-averaged snapshots of a single wind turbine LES in a coastal LLJ (a,c) and MS (baseline) (b,d). (a), (b) time-averaged (20 min) wind-speed. (c), (d) resolved TKE, $\frac{1}{2}(\overline{u'^2 + v'^2 + w'^2})$

3.3. Turbine response: single turbine simulations

In the present section, we describe fatigue damage on a turbine in terms of the damage equivalent loads (DEL) [16], calculated from stress reversals. Note, for the blades, a wohler exponent of 12 has been used whereas for the hub and tower a wohler exponent of 4 has been used; these are consistent with the previous literature [17]. Table 3 shows that the damage equivalent edgewise and the flapwise blade moments are comparable in both the baseline MS and coastal LLJ owing to comparable wind speeds and comparable TI in the rotor region. The major differences occur in the hub center loads, e.g., the yaw bearing and low-speed shaft loads, where more than 15% increment in loads are predicted in the LLJ cases primarily due to the strong veer in the winds.

The presence of veer and wind turbulence also causes $\sim 40\%$ increment in the tower side–side loads and $\sim 17\%$ increment in the tower twisting loads.

Case	*RootMxb1*	*RootMyb1*	*YawBrMxn*	*YawBrMyn*	*YawBrMzp*	*LSSTipMys*	*LSSTipMzs*	*TwrBsMxt*	*TwrBsMyt*	*TwrBsMzt*
-	[kN-m]	[kN-m]	[kN-m]	[kN-m]	[kN-m]	[kN-m]	[kN-m]	[kN-m]	[kN-m]	
MS	9362.53	6525.47	32.204	279.64	261.18	264.17	261.15	557.13	537.55	261.16
LLJ	9397.29	6361.44	48.66	323.64	316.84	296.11	309.689	1050.36	607.94	316.85
% diff	+0.3699	-2.578	+33.828	+13.595	+17.566	+10.786	+15.672	+46.95	+11.57	+17.57

Table 3: Comparison of damage equivalent loads (DEL) of blade roots and yaw bearing and hub moments of a single wind turbine LES in the baseline MS and coastal LLJ. RootMxb1 – Edgewise moment, RootMyb1 – Flapwise moment, YawBrMxn – Yaw bearing roll moment, YawBrMyn – Yaw bearing pitch moment, YawBrMzp - Yaw bearing yaw moment, LSSTipMys , LSSTipMzs – low-speed shaft/ hub moments, TwrBsMxt – Side-side moment, TwrBsMyt – Fore-aft moment and TwrBsMzt - Tower twisting moment.

Case	*GenPwr*	*GenSpeed*	*RotThrust*	*RotTorq*	*RtVAvgxh*
-	[kW]	[rpm]	[kN]	[kN-m]	[m/s]
MS	14997.6 (230.40)	7.55 (0.116)	2067.75 (179.36)	19623.91 (28.84)	10.25 (0.85)
LLJ	15002.19 (180.92)	7.56 (0.09)	2176.49 (149.58)	19623.99 (37.16)	9.50 (0.59)
% diff	0.03 (-27.34)	0.03 (-27.35)	+4.99 (-19.90)	0.0003 (22.37)	-7.87 (-45.38)

Table 4: Comparison of mean generator power (GenPwr), generator speed (GenSpeed), Rotor Thrust (RotThrust), Rotor Torque (RotTorq) and Rotor averaged velocity (RtVAvgxh) in the baseline MS and coastal LLJ.% difference of both mean and standard deviations (in parentheses) are recorded (last 10 min. of 20 min. simulations)

We also compare the rotor-averaged loads, velocity, generator power and rotor speed (RPM) for the two ABL cases. Owing to similar hub-height wind, the mean generator power and RPM between the two cases are very similar ($< 0.1\%$ difference). However, the standard deviations in the generator power and RPM of the LLJ case are significantly lower than the MS case ($\sim 30\%$). The LLJ have $30-50\%$ higher TI_{IEC} than the MS case in the rotor region. Thus, the reduction in variability in the generator power and generator speed can be attributed to stability of the ABL. Additionally, the rotor averaged velocity in the coastal LLJ case is $\sim 8\%$ lower than the MS case demonstrating that the strong induction effect upstream of the turbine is primarily influenced by the shallow stable layer in LLJ accompanied by the lack of turbulent mixing.. While this is not critical for a single turbine, the induction losses can propagate upstream to larger blockage losses for large wind turbine arrays resulting in loss of generator power.

3.4. Wind turbine Array

In this section, we discuss the wind turbine array simulations (5×4 layout) driven by the ABL precursor as inflow conditions. The turbines are separated by $5D$ in the dominant wind direction and $4D$ in the lateral direction. Figure 6 shows the wake propagation of the wind farm array for the MS and LLJ cases. The most evident effect in the turbine simulations are the presence of deeper farm wakes due to the wake superposition of turbines in the downstream direction as also observed in the author's high-fidelity spectral-element simulations of neutral boundary layer of wind farms [14, 15]. As seen in the single turbine case, the wakes are also deeper in the 20-turbine cases with significant amount of dispersion (owing to veering) for the LLJ compared

to the MS cases, as clearly illustrated by the time-averaged plots in Figure 7. The deeper wakes in the LLJ cases propagate downstream, which have detrimental consequences on the turbine hub loads compared to the MS cases.

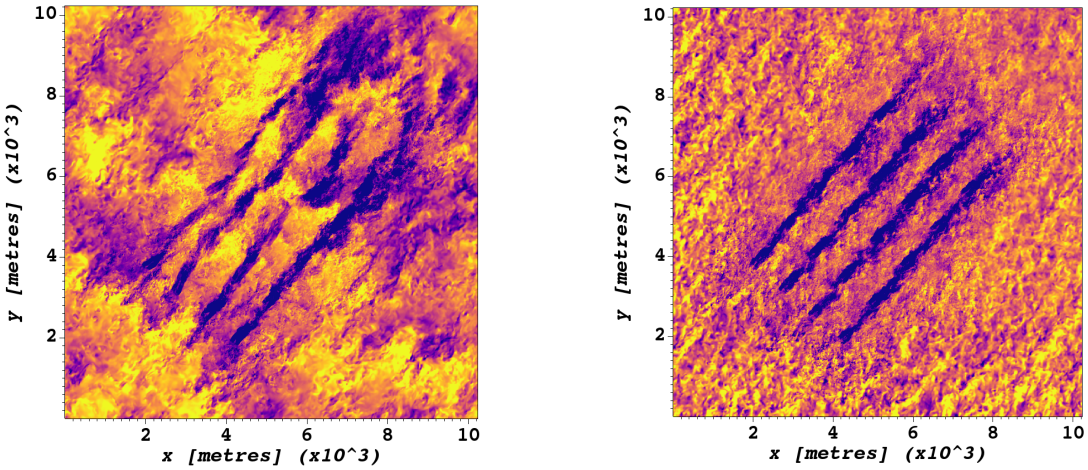

Figure 6: Comparison of instantaneous snapshots (planform view) of wind farm (5×4 layout) in MS (a) and coastal LLJ (b). Colormap and timestamp same as in Figure 4.

In addition to wake deficits, Figure 7 also indicates that the induction losses are deeper in the LLJ case compared to the MS case. Additionally, we also observe augmentation of the turbulence (resolved TKE) near the top-tip location due to the wakes (more in the MS cases than the LLJ cases) which further propagates downstream. We also documented the growth of the internal boundary layer in the MS case, owing to the entertainment of the outer layer due to wake augmented turbulence, but in the LLJ case the wake turbulence is completely trapped under the capping inversion layer.

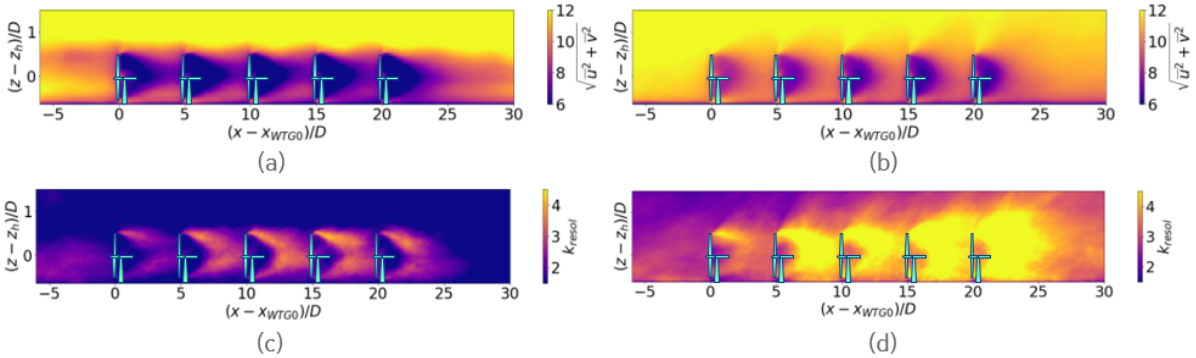

Figure 7: Comparison of time-averaged snapshots of a 20 turbine wind farm LES in a coastal LLJ (a,c) and MS (baseline) (b,d). (a), (b) time-averaged (20 min) wind-speed. (c), (d) resolved TKE, $\frac{1}{2}(\overline{u'^2} + \overline{v'^2} + \overline{w'^2})$. The results are averaged over the 4 lateral planes containing 5 turbines each.

3.5. Turbine response: Wind turbine Array

In this section, we discuss the turbine response observed in the 20 wind turbine (5×4 layout) simulation. In Figure 8, we observe that the edgewise moments decrease across rows (in the streamwise direction) and turbine hub loads are shown to progressively increase across rows. Despite an increased turbulence in the downstream turbines, the decrease in the blade edgewise loads in the LLJ compared to the MS case could potentially be attributed to the lower wind speeds (stronger wakes) and lower wake-augmented turbulence. Additionally, the increased hub and tower twist loads in the LLJ case are a testimony of a combined effect of increased turbulence and increased wind veer in the downstream turbines. Figure 8b shows the yaw bearing yawing moment ($YawBrMzp$), but similar trends between the MS and LLJ cases are also observed for the hub/low-speed shaft loads ($LSSTipMys, LSSTipMzs$). Further, Figures 8c , 8d illustrate non-monotonic trends in the side–side moments due to combined effect of veer and turbulence while the twisting moments in the downstream turbines increase in the LLJ case primarily due to veer. Finally, in Figure 8e, 8f we observe that the power downstream of the turbines drop significantly e.g., $\sim 50\%$ in the LLJ case owing to the strong wake deficits compared to $< 10\%$ drop in power in the MS cases. This is accompanied by the drop in rotor thrust in LLJ event compared to MS. Since the wakes recover quickly in the MS case, a significant row-wise variation of the rotor thrust is not observed for the MS case. Further, we observe that the standard deviation of the generator power and rotor thrust increase downstream of turbines (more in the MS case) concomitant with wake turbulence intensity of the farms.

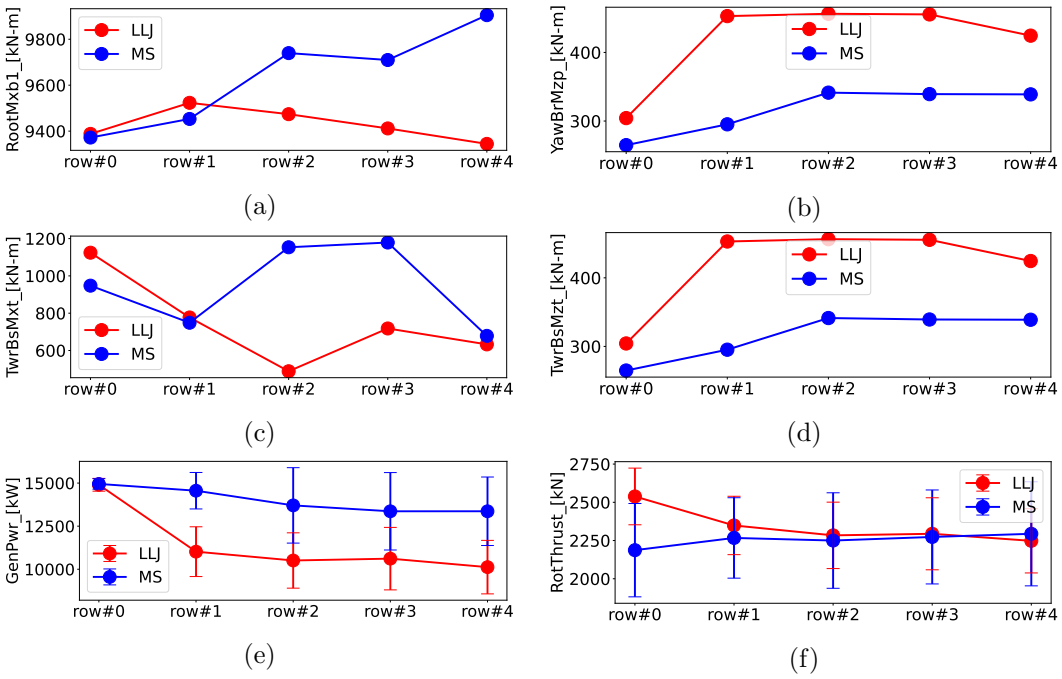

Figure 8: Comparison of row-wise variation of damage equivalent loads (DEL) of blade edgewise, turbine hub, tower and mean and standard deviation of generator power, rotor thrust of the wind farm array LES in the baseline MS and coastal LLJ case. Label same as in Table 3. The mean, standard deviation and DEL data are averaged across 4 arrays of turbines.

4. Discussion and Future Work

In the present work, we demonstrate the impacts of coastal LLJ events in turbines and compare it against monotonically sheared convectively unstable boundary layer (with similar

wind conditions) using high-fidelity aeroelastic solver coupled LES. The results indicate that the *strong veer* in LLJ have significant increase in the damage equivalent hub-loads and tower loads ($20-40\%$) both for single turbine and wind farms. For the wind farm case, the downstream propagating strong wake deficit region with reduced wake turbulence for the LLJ event contributes to the decrements of the edgewise loads, generator power along with the rotor thrust. The wind farm case further illustrates that the findings from the single-turbine blade, tower, hub-load and power analyses may not be directly translatable to the farm case. The study indicates that since the occurrence of LLJ events are infrequent ($2-7\%$ in a year), the drop in power during the LLJ event is perhaps not critical towards contributing to a significant net drop in AEP as are the increments of DEL hub and tower loads. The blades and tower loads for both MS and LLJ cases are within the design envelopes obtained from design load condition (DLC) simulations [10]. Design envelopes for the hub-loads based on DLC simulations currently do not exist, which indicates that incorporation and standardization of hub loads (yaw bearing and low speed shaft) in DLC analysis might be necessary to consider non conventional wind events like LLJ. This study provides a foundation to understand potential avenues to mitigate turbine loads due to LLJ events for future exploration using active load control. Finally, the current study involved comparison of LLJ against an unstable simulation with similar wind speed, direction and TI at hub-height but different turbulent coherent structures, wind veer and shear. As a next step, we would also compare the LLJ case against a conventional stable boundary layer with similar turbulent structures, wind veer and rotor-averaged sheer which would potentially shed light on the impact of LLJ turbulent structures on the turbine loads.

5. Acknowledgment

This material is based upon work supported by the U.S. Department of Energy's Office of Energy Efficiency and Renewable Energy (EERE) under the Wind Energy Technologies Office Award Number DE-EE0008390. This report was prepared as an account of work sponsored by an agency of the United States Government. Neither the United States Government nor any agency thereof, nor any of their employees, makes any warranty, express or implied, or assumes any legal liability or responsibility for the accuracy, completeness, or usefulness of any information, apparatus, product, or process disclosed, or represents that its use would not infringe privately owned rights. Reference herein to any specific commercial product, process, or service by trade name, trademark, manufacturer, or otherwise does not necessarily constitute or imply its endorsement, recommendation, or favoring by the United States Government or any agency thereof. The views and opinions of authors expressed herein do not necessarily state or reflect those of the United States Government or any agency thereof.This work was authored in part by the National Renewable Energy Laboratory, operated by Alliance for Sustainable Energy, LLC, for the U.S. Department of Energy (DOE) under Contract No. DE-AC36-08GO28308. Funding provided by the U.S. Department of Energy Office of Energy Efficiency and Renewable Energy Wind Energy Technologies Office. The views expressed in the article do not necessarily represent the views of the DOE or the U.S. Government. The U.S. Government retains and the publisher, by accepting the article for publication, acknowledges that the U.S. Government retains a nonexclusive, paid-up, irrevocable, worldwide license to publish or reproduce the published form of this work, or allow others to do so, for U.S. Government purposes.This research used resources of the Oak Ridge Leadership Computing Facility, which is a DOE Office of Science User Facility supported under Contract DE-AC05-00OR22725.

References

[1] Adam W Lavely, Ganesh Vijayakumar, Brent Craven, Balaji Jayaraman, Eric G Paterson, Tarak N Nandi, and James Brasseur. Towards a blade-resolved hybrid urans-les of the nrel 5-mw wind turbine rotor within large eddy simulation of the atmospheric boundary layer. In *32nd ASME Wind Energy Symposium*, page 0869, 2014.

[2] Ganesh Vijayakumar, James Brasseur, Adam W Lavely, Balaji Jayaraman, and Brent Craven. Interaction of atmospheric turbulence with blade boundary layer dynamics on a 5mw wind turbine using blade-boundary-layer-resolved cfd with hybrid urans-les. In *34th Wind Energy Symposium*, page 0521, 2016.

[3] Balaji Jayaraman and James G Brasseur. The surprising transition in atmospheric boundary layer turbulence structure from neutral to moderately convective stability states and mechanisms underlying large-scale rolls. *arXiv preprint arXiv:1807.03336*, 2018.
[4] David J. Stensrud. Importance of low-level jets to climate: A review. *Journal of Climate*, 9(8):1698 – 1711, 1996.
[5] Jeanie A. Aird, Rebecca J. Barthelmie, Tristan J. Shepherd, and Sara C. Pryor. Occurrence of low-level jets over the eastern u.s. coastal zone at heights relevant to wind energy. *Energies*, 15(2), 2022.
[6] Michael Sprague, S Ananthan, G Vijayakumar, and M Robinson. A new $k-\epsilon$ model consistent with monin-obukov similarity theory. *Wind Energy*, 20:479–289, 2017.
[7] Srinidhi N. Gadde and Richard J. A. M. Stevens. Effect of low-level jet height on wind farm performance. *Journal of Renewable and Sustainable Energy*, 13(1):013305, 2021.
[8] Michael Sprague, S Ananthan, G Vijayakumar, and M Robinson. Exawind: A multifidelity modeling and simulation environment for wind energy. *Journal of Physics: Conference Series*, 1452:012071, 01 2020.
[9] DNV-GL. Nyserda floating lidar buoy data, 2020. online.
[10] E. Gaertner et al. Definition of the iea 15-megawatt offshore reference wind turbine, 2020. online.
[11] D. Allaerts, E. Quon, C. Draxl, and M. Churchfield. Development of a time–height profile assimilation technique for large-eddy simulation. *Boundary Layer-meteorology*, 176:329–348, 2020.
[12] M. Optis, N. Bodini, M. Debnath, and P. Doubrawa. New methods to improve the vertical extrapolation of near-surface offshore wind speeds. *Wind Energy Science*, 6(3):935–948, 2021.
[13] S. E. Haupt et al. First-year report of the atmosphere to electrons mesoscale-to-microscale coupling project, 2015. PNNL - 25108.
[14] Tanmoy Chatterjee and Yulia T. Peet. Dynamics of large scale turbulence in finite-sized wind farm canopy using proper orthogonal decomposition and a novel fourier-pod framework. *Energies*, 13(7), 2020.
[15] Tanmoy Chatterjee and Yulia T. Peet. Streamwise inhomogeneity of spectra and vertical coherence of turbulent motions in a finite-size wind farm. *Phys. Rev. Fluids*, 6:114601, Nov 2021.
[16] René M.M. Slot, John D. Sørensen, Lasse Svenningsen, Wolfgang Moser, and Morten L. Thøgersen. Effective turbulence and its implications in wind turbine fatigue assessment. *Wind Energy*, 22(12):1699–1715, 2019.
[17] R. Kazacoks and P. Jamieson. Evaluation of fatigue loads of horizontal up-scaled wind turbines. *Energy Procedia*, 80:13–20, 2015.